Multiscale Modeling of Thermoplastics Using Atomistic-informed Micromechanics

Evan J. Pineda[1]
NASA Glenn Research Center, Cleveland, OH, 44135, U.S.A.

Jamal F. Husseini[2]
University of Massachusetts, Lowell, MA, 01854, U.S.A.

Joshua D. Kemppainen[3]
Michigan Technological University, Houghton, MI, 49931, U.S.A.

Brett A. Bednarcyk[4]
NASA Glenn Research Center, Cleveland, OH, 44135, U.S.A.

William A. Pisani[5]
Oak Ridge Institute for Science and Education, Oak Ridge, TN, 37830, U.S.A
U.S. Army Engineer Research and Development Center, Vicksburg, MS, 39180, U.S.A.

Gregory M. Odegard[6]
Michigan Technological University, Houghton, MI, 49931, U.S.A.

Scott E. Stapleton[7]
University of Massachusetts, Lowell, MA, 01854, U.S.A.

[1] Research Aerospace Engineer, Multiscale and Multiphysics Modeling Branch, AIAA Associate Fellow.
[2] NASA Space Technology Research Grant Opportunity Fellow, Dept. of Mechanical Engineering, AIAA Member.
[3] Graduate Research Assistant, Dept. of Mechanical Engineering-Engineering Mechanics.
[4] Research Materials Engineer, Multiscale and Multiphysics Modeling Branch, AIAA Associate Fellow.
[5] ORISE Postdoctoral Fellow, Environmental Laboratory.
[6] John O. Hallquist Endowed Chair, Dept. of Mechanical Engineering-Engineering Mechanics, AIAA Associate Fellow.
[7] Associate Professor, Dept. of Mechanical Engineering, AIAA Member.

A multiscale model was developed for predicting the thermoelastic behavior of semi-crystalline thermoplastic materials for composite aerospace applications. At the highest scale containing the semi-crystalline spherulite in an amorphous matrix, the generalized method of cells, or high fidelity method of cells, was used to perform the homogenization calculations to obtain the effective properties. Models were developed assuming a cubic, or spherical shape, for the spherulite to understand if the morphology of the spherulite affects the effective thermoelastic properties. The generalized method of cells was used to model at the repeating unit cells at the subscales of the microstructure including the lamellae stacks and granular crystal blocks. The scales are integrated using the multiscale micromechanics method in the NASA Multiscale Analysis Tool. Data from molecular dynamics simulations were used as inputs for the amorphous and crystalline constituents. Convergence studies were performed to determine the best level of discretization for the repeating unit cell at the highest scale. Effective Young's modulus, shear modulus, Poisson's ratio, coefficient of thermal expansion, and thermal conductivity were predicted for polyether ether ketone and polyether ketone ketone, and very good agreement between the model utilizing the cubic spherulite and the experimental data, where available, was observed for polyether ketone ketone. Normalization of the data for the bulk polyether ketone ketone, against amorphous data, improved the predictions as compared to experimental data. Overall, the high fidelity method of cells predicted a stiffer response then the generalized method of cells as the crystallinity was increased. The shape of the spherulite had a minimal effect on the predicted bulk properties of the polymers.

I. Introduction

Thermoplastic materials, including polyether ether ketone (PEEK) and polyether ketone ketone (PEKK) are high-performance semi-crystalline polymers ideal for aerospace applications because of their excellent properties, toughness, resistance to aging, manufacturability and "tailorability." The increase in interest in these materials for is evident by several new NASA projects that have been recently established focused on the use of thermoplastic composites for both aeronautics and space applications. To design improved composite matrix materials incorporating thermoplastics, a thorough understanding of the coupling between the molecular structure, continuum-level microstructure, and the resulting bulk response of the thermoplastics is imperative.

Limited research has been performed to understand the influence of the molecular structure on bulk material properties. A recent review paper collected information on the morphology of neat PEEK and PEKK near a carbon fiber interface and the influence of crystallinity on Young's modulus [1]. Wherever relevant, comparisons of PEKK to the more extensively studied PEEK were drawn. Talbott et al. demonstrated experimentally that Young's modulus, shear modulus, tensile yield strength, and shear yield strength increase as the relative crystalline content of PEEK increases [2]. Talbott et al. also determined by X-ray scans that the crystalline structure deteriorates significantly (~10% drop in crystallinity) when the applied compression loading increases beyond the yield point [2]. More recently, similar measurements have been made for PEKK [3] Despite these initial efforts, more experimental research is needed to provide a better understanding of the effect of molecular structure on bulk properties of PEKK and PEEK.

Computational simulation techniques can also be used to establish structure-property relationships for thermoplastic materials and supplement experimental data. Specifically, molecular dynamics (MD) simulation techniques are well-suited for predicting bulk-level properties of single-phase polymers based on molecular structure [4-5]. However, MD simulation techniques alone cannot predict the bulk level properties of semi-crystalline materials because the characteristic length scale (i.e., crystallites) of these materials (microns) is orders of magnitude larger than those that can be efficiently simulated with fully atomistic MD models (nanometers). To effectively simulate semi-crystalline polymer materials, a multi-scale approach can be used in which the amorphous and crystalline phases are modeled separately using MD, and micromechanics is subsequently used to obtain the bulk properties using repeating unit cells (RUCs) that represent the spatial arrangement of these phases at larger length scales. Developing an integrated framework allows for engineers to both design with the material and design the material itself, a key aspect of Integrated Computational Materials Engineering (ICME).

An early multiscale model for thermoplastic composites was presented by Chapman et al. to examine residual stresses in carbon/PEEK laminates [6]. At the crystalline/amorphous scale in the PEEK matrix, this work employed the micromechanics model of Ogale and McCullough, which considered the aspect ratio and a random orientation of the crystalline phase [7]. Based on these homogenized PEEK matrix properties, Chapman et al. [6] then used rule of

mixtures type models for the unidirectional ply (including viscoelastic effects in the transverse direction) and lamination theory to obtain the macroscale laminate thermo-mechanical response. In more recent years, there have been several analytical micromechanics models presented in the literature for predicting the properties and response of semicrystalline thermoplastics based on the properties of the amorphous and crystalline constituent phases. For example, Guan and Pitchumani used an ellipsoidal Mori-Tanaka micromechanics model to predict the Young's moduli of semicrystalline polyethylene and syndiotactic polystyrene as a function of crystallinity [8]. Their results showed the importance of capturing the semicrystalline microstructure for predicting accurate elastic properties. Bédoui and co-workers used several classical micromechanics homogenization methods to predict the effective elastic properties of semicrystalline isotactic polypropylene, polyethylene, and polyethylene terephthalate (PET) [9]. They then extended this investigation to consider the viscoelastic behavior of PET in ref. [10]. Gueguen et al. compared Mori-Tanaka, double-inclusion, and self-consistent micromechanics models for predicting the elastic properties of semicrystalline polyethylene based on the amorphous and crystalline phases [11]. Glüge et al. used an uncoupled, two-step homogenization approach, including orientational averaging, to predict the effective Young's modulus of semicrystalline isotactic polypropylene as a function of crystallinity [12]. van Dommelen et al. extended existing micromechanics methods to include viscoplasticity and large deformations to investigate the response of high-density polyethylene and PET [13].

The literature indicates that more emphasis has been placed on analytical and semi-analytical micromechanics models for semicrystalline thermoplastics as opposed to numerical, finite element method (FEM) models. Examples of FEM-based micromechanics models for semicrystalline thermoplastics include the work of Hsia et al. [14], Doyle [15], and Poluektov [16]. Of course, this approach requires meshing of the microstructure and tends to be more computationally demanding, particularly when considering multiple scales. Finally, Jin et al. [17], in addition to presenting a comprehensive investigation of PEEK semicrystalline microstructure, developed a relevant MD model of the crystalline phase that incorporated imperfections.

It has been demonstrated previously that MD modeling coupled hierarchically with the multiscale generalized method of cells (MsGMC) can be used to accurately predict the mechanical properties of semi-crystalline PEEK [18, 19]. These papers presented the methodology for establishing well-equilibrated amorphous and crystalline PEEK MD models with the Reactive Force Field (ReaxFF) [20], as well as the procedure for predicting the mechanical response of each phase at the molecular level. The crystalline PEEK MD results were compared with density functional theory (DFT) results for validation. This study also presented the methodology for modeling the semi-crystalline structure of PEEK with the multiscale generalized method of cells (MsGMC) module of the NASA Micromechanics Analysis Code/Generalized Method of Cells (MAC/GMC) using the simulated molecular response as input [21, 22]. Following this, the predicted mechanical properties were compared to experiment for model validation for one value of crystallinity. The developed multiscale modeling methodology was later extended to other semi-crystalline polyamide 6 [23].

The multiscale continuum model for the semi-crystalline spherulite has been further developed using the multiscale recursive micromechanics (MsRM) framework within the NASA Multiscale Analysis Tool (NASMAT) software package [24, 25]. The MsRM framework within NASMAT offers more flexibility because than MsGMC in MAC/GMC because it allows for any micromechanics theory to be deployed at any scale in an integrated (two-way coupling) fashion. Thus, the high fidelity generalized method of cells (HFGMC) can be utilized at the highest scale to capture the local fields arising from the presence of a spherical inclusion more accurately, while the generalized method of cells (GMC) can be retained for all additional subscales. Moreover, the original MsGMC model utilized a cubic shape for the spherulite. With GMC, the sharp corners of the cubic inclusion do not influence the local fields. However, these stress concentrations are captured with HFGMC. Therefore, a spherical model for the spherulite was also developed. Finally, to predict the effective thermal conductivity of semi-crystalline materials, a generalized HFGMC solution for physics governed by vector-based constitutive laws has been implemented into MsRM within NASMAT [26]. Inputs for the constituent properties are obtained from MD results from Pisani, et al. (PEEK), and more recently, Kemppainen et al. (PEKK) [18, 27]. The work presented here represents a purely computational workflow for predicting effective thermoelastic properties, and it is validated against experimental data where available.

The focus of the current work is to evaluate the different MsRM modeling strategies for their ability to predictive effective thermoelastic properties of semi-crystalline thermoplastics. As such, it is also important to understand modeling requirements, theoretical restrictions, and computational performance of the models. The current paper is arranged as such. A summary of the HFGMC homogenization for physics governed by vectorized constitutive laws is given in Section II. Details on the MsRM model for the spherulite are given in Section III. Model verification and results from studies on the convergence of properties as a function of discretization are presented in Section IV. The

predicted stiffness, coefficient of thermal expansion (CTE), thermal conductivity properties for PEEK and PEKK as a function of crystallinity are presented in Section V, followed by conclusions in Section VI.

II. Generalized HFGMC Solution for Physics Governed by Vector-based Constitutive Law

A new version of the HFGMC micromechanics theory was developed for many different physical phenomena governed by vector constitutive laws in Bednarcyk, et al. in composite materials [26]. This enabled, in addition to the standard mechanical problem, (1) homogenization to obtain effective composite properties and (2) localization to obtain local field quantities for thermal and electrical conductivity problems, magnetic permeability problems, diffusion problems, and problems involving fluid flow through a porous medium. The constitutive equations for all these physical phenomena can be written in a common form as,

$$\mathbf{Y} = -\mathbf{Z}\nabla\psi = \mathbf{Z}\,\mathbf{X} \tag{1}$$

where, for example, in the case of the thermal conductivity problem, this represents Fourier's Law,

$$\mathbf{q} = -\boldsymbol{\kappa}\nabla T \tag{2}$$

where $\mathbf{q}$ is the heat flux vector, $\boldsymbol{\kappa}$ is the second-order thermal conductivity tensor, and T is the temperature, so,

$$\mathbf{Y} = \mathbf{q}, \qquad \psi = T, \qquad \mathbf{Z} = \boldsymbol{\kappa}, \qquad \mathbf{X} = -\nabla T \tag{3}$$

Similar analogies can be made for all the physics described above, and, by simply using the correct input properties for the constituent materials, the effective composite properties associated with any of the physics can be determined via the HFGMC homogenization procedure. Likewise, by considering application of the appropriate global field quantities (for example, global composite heat fluxes), the local field quantities for any of the physics can also be determined by HFGMC (for example, the local heat fluxes and temperature gradients in the constituents throughout the composite). $\mathbf{Z}$ thus represents a general property tensor, while $\mathbf{Y}$ and $\mathbf{X}$ are the field variable vectors. Note that, for all the physics, the governing equation is given by,

$$\nabla \cdot \mathbf{Y} = 0 \tag{4}$$

In MsRM, see Fig. 1, the scales are linked by equilibrating the homogenized fields and properties (global strain, stress, and stiffness tensors for the mechanical problem and global temperature gradient, heat flux, and thermal conductivity tensors for the thermal problem, for example) at level i to the analogous local fields and properties of a given sub-volume at level i (with appropriate transformation to account for the potential coordinate system change from scale to scale). Hence, starting with the lowest scale (k) microstructure (see Fig. 1), whose sub-volumes contain only monolithic materials, the effective stiffness ($\mathbf{C}$) or multiple physics property ($\mathbf{Z}$) tensors can be calculated. This stiffness or property tensor (after appropriate coordinate transformation) then represents the homogenized material occupying one of the sub-volumes within a composite material at the next higher length scale. Given the transformed effective stiffness ($\mathbf{C}$) or property ($\mathbf{Z}$) tensors of all sub-volumes at this next higher length scale, the effective stiffness and property tensors of the composite at this level can be determined. These stiffness and property tensors can then be transformed and passed along to the next higher length scale, and the process repeats until the highest length scale considered (0) is reached.

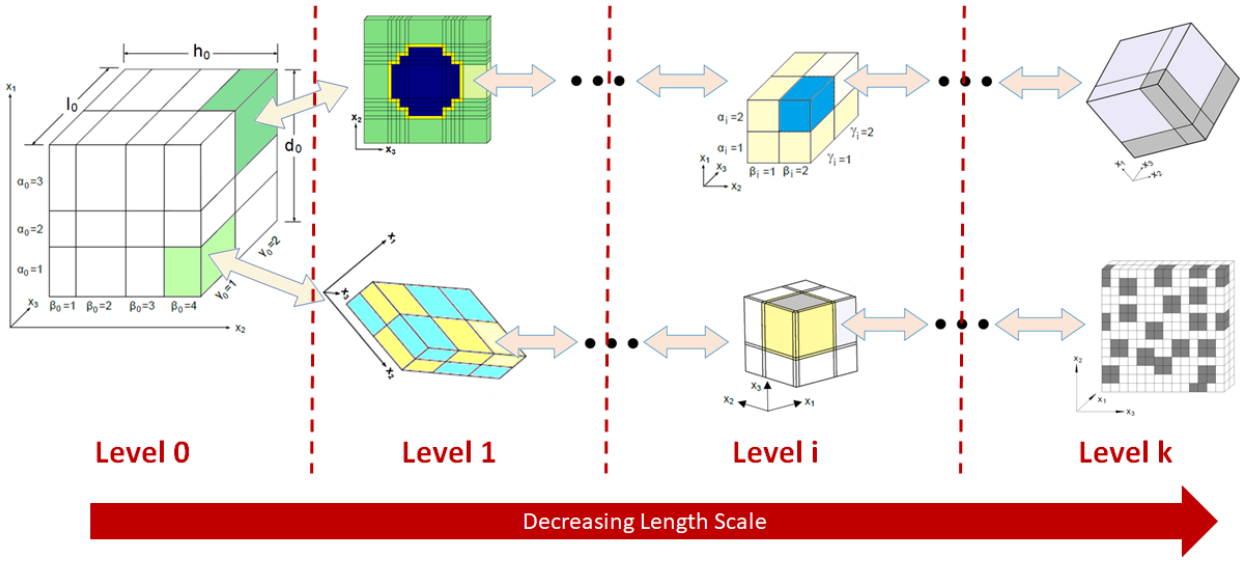

Fig. 1 MsRM integrated hierarchy linking repeating unit cells (RUCs) and subcells across an arbitrary number of length scales.

As an example, for an MsRM analysis considering three length scales (0, 1, and 2), the overall effective stiffness tensor can be written as,

$$\mathbf{C}_0^* = \sum_{\alpha_0} v_{\alpha_0} \left\{ \left(\mathbf{T}_4^1\right)^{-1} \sum_{\alpha_1} v_{\alpha_1} \left[\left(\mathbf{T}_4^2\right)^{-1} \sum_{\alpha_2} v_{\alpha_2} \mathbf{C}_2^{(\alpha_2)} \mathbf{A}_2^{M(\alpha_2)} \right]^{(\alpha_1)} \mathbf{A}_1^{M(\alpha_1)} \right\}^{(\alpha_0)} \mathbf{A}_0^{M(\alpha_0)} \tag{5}$$

whereas the effective property tensor can be written as,

$$\mathbf{Z}_0^* = \sum_{\alpha_0} v_{\alpha_0} \left\{ \left(\mathbf{T}_2^1\right)^{-1} \sum_{\alpha_1} v_{\alpha_1} \left[\left(\mathbf{T}_2^2\right)^{-1} \sum_{\alpha_2} v_{\alpha_2} \mathbf{Z}_2^{(\alpha_2)} \mathbf{A}_2^{MP(\alpha_2)} \right]^{(\alpha_1)} \mathbf{A}_1^{MP(\alpha_1)} \right\}^{(\alpha_0)} \mathbf{A}_0^{MP(\alpha_0)} \tag{6}$$

Here, $\mathbf{A}_i^{M(\alpha_i)}$ and $\mathbf{A}_i^{MP(\alpha_i)}$ are the mechanical problem and multiple physics problem concentration tensors, respectively, $\mathbf{T}_2^i$ and $\mathbf{T}_4^i$ are the appropriate second and fourth order coordinate transformation matrices, v_{α_i} is the volume fraction of sub-volume α_i, and $\mathbf{C}_i^{(\alpha_i)}$ and $\mathbf{Z}_i^{(\alpha_i)}$ are the stiffness and property tensors of sub-volume α_i at level *i*. Note that in Eqs. (5) and (6), the superscript on the bracketed terms indicates that all variables within the brackets are a function of the sub-volume indices from the next higher length scale (including lower scale volume fractions and sub-volume indices). The intent of this notation is to fully define the sub-volume at a given scale as one progresses down the length scales.

Converse to this multiscale homogenization procedure, MsRM performs multiscale localization of the strain and stress tensors or the **Y** and **X** field variable vectors. The multiscale localization is needed to calculate the strain, stress, and multiple physics fields at all length scales using a variety of micromechanics theories (see refs. [24, 25, 28-30] for details).

III. Multiscale Recursive Micromechanics Model for Semi-crystalline Thermoplastics

A. Hierarchy of multiscale model

The morphological hierarchy for a RUC, and the MsRM strategy used to calculate the effective thermoelastic properties, of a thermoplastic material is shown in Fig. 2. Four disparate length scales, Levels 0 (highest) – 3(lowest) are explicitly considered. Superscripts indicate the associated level and subscripts indicate the specific local material coordinate frame. The crystalline and amorphous regions of Level 3 were assigned the properties obtained from MD data, see Section V.B [18, 27]. The elastic properties of the granular crystal block (GCB), lamellae stacks, and spherulite are integrated using MsRM in NASMAT. GMC is used to model the GCB (Level 2) and lamellae stacks (Level 1) with two subcells by two subcells doubly periodic RUCs containing a crystalline subcell surrounded by three amorphous subcells. Seminal work in the development of this model utilized GMC at Level 0 to model the spherulite and assumed a cubic shape because the lack of normal-shear coupling which can result in deficiencies in the accuracy of the local fields when the reinforcements are discontinuous [18, 32]. This strategy works well for predicting effective properties. However, with an eye towards predicting material nonlinearity, the current work also utilizes HFGMC to perform the homogenization at Level 0. The normal-shear coupling retained with HFGMC introduces stress concentrations at sharp corners, similar to FEM. Thus, the inclusion was modeled as a voxelized sphere, as shown in Fig. 2. For consistency, an MsRM model containing a spherical spherulite analyzed with GMC was also considered. A convergence study, discussed in Section III.B, was performed to determine the discretization requirements N for the Level 0 triply periodic (GMC or HFGMC) RUCs. A summary of the models used to generate results for PEKK and PEEK in this work is summarized in Table 1. The results are presented and discussed in Sections IV and V to assess the predictive capabilities, modeling requirements, theoretical restrictions, and computational performance of the different models before moving forward with more involved nonlinear simulations.

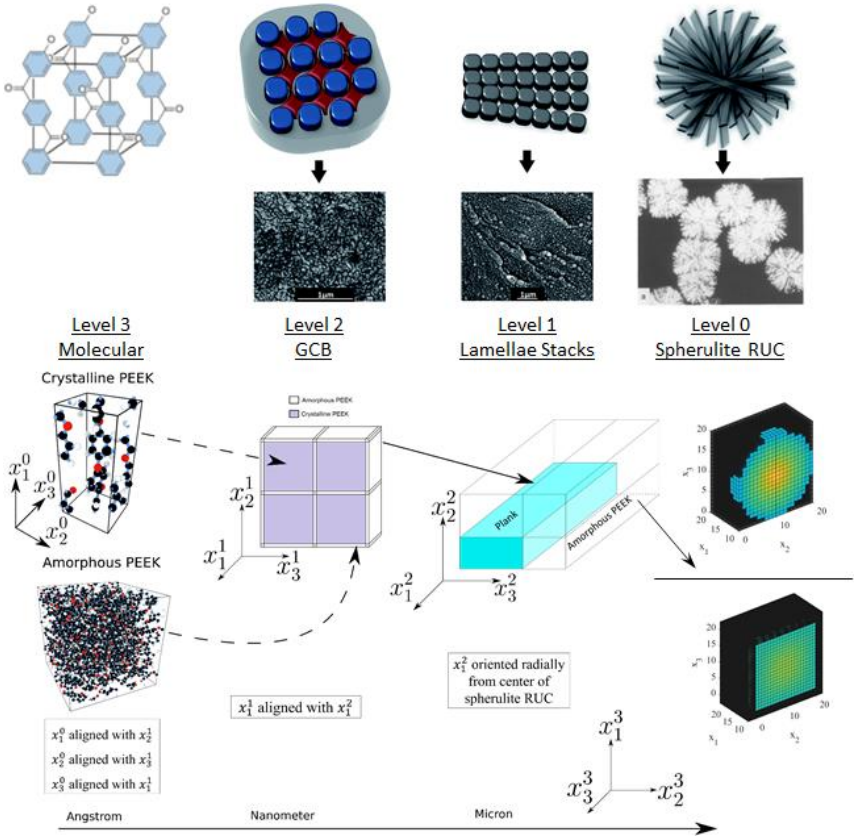

Fig. 2 Hierarchy of relevant length scales present in a thermoplastic material. The top row shows images of the geometric approximations and experimental images at each scale, while the bottom row displays the computational model [1, 18]. Superscripts indicate the associated level and subscripts indicate the specific axis.

Table 1. Summary of MsRM models.

Material	Shape of Spherulite	Level 0 Micromechanics Theory
PEEK/PEKK	Sphere	GMC
PEEK/PEKK	Sphere	HFGMC
PEEK/PEKK	Cube	GMC
PEEK/PEKK	Cube	HFGMC

The lamellae stacks in the spherulite grow radially outward from the nucleation site as the material is held at the crystallization temperature, see Fig. 2 [1]. The spherulites exist in an amorphous matrix phase which also occupies the volume between the lamella stacks. The amount of inter-spherulite matrix is dependent on how long the material is held at the crystallization temperature [32]. Manufacturing processes, such as annealing and quenching, may be utilized to control the overall crystallinity and morphology. To accurately predict the thermoelastic properties as function of the material microstructure, it is important the local crystallinity within the domain of the spherulite v_c and the overall crystallinity χ are approximated well in the multiscale model.

To achieve this for the spherical model, it was assumed the core of the spherulite has a local crystallinity of 0.85, which was estimated based upon the 0.862 crystallinity of the GCB v_{GCB} [18]. Then, the density of the lamellae stacks, or local crystalline volume fraction v_c, decreases in subcells as the radial distance from the center of the RUC increases. Figure 3 shows the algorithm used to generate the MsRM model and write the NASMAT input file. The cubic model is based upon previous work. For details on that algorithm, the reader is referred to Ref. [18].

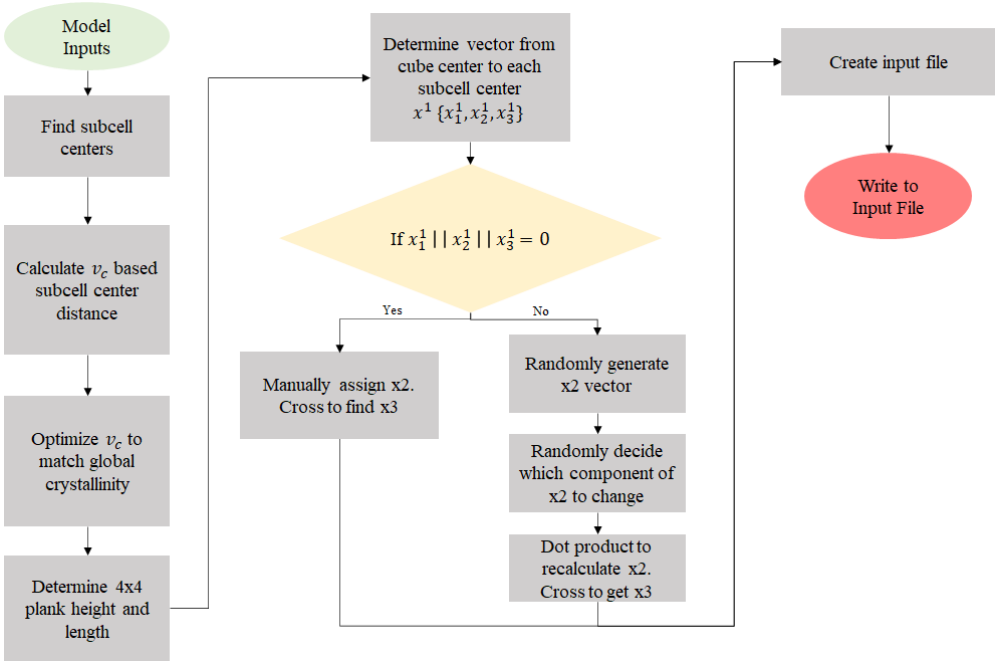

Fig. 3 Algorithm for constructing the MsRM model and writing the NASMAT input file.

B. Modeling inputs

Inputs for the constituent properties (amorphous and crystalline phases) of the models were obtained from MD [18, 19, 27]. Thus, the predictions shown in Section V are obtained purely via simulation and did not utilize any

experimental data or calibration. PEKK T/I 70/30 was modeled using IFF/IFF-R (Interface Force Field/Reactive Interface Force Field). The amorphous phase and crystalline phase were modeled and characterized separately with the intention to homogenize using NASMAT. All the MD simulations were performed in LAMMPS June 23rd, 2022, software. The amorphous phase models were polymerized using the LAMMPS *fix bond/react* command, in conjunction will LAMMPS molecule templates to superimpose bonded geometry changes. During the polymerization water by-products were produced and removed immediately. The optional *fix bond/react inter* flag was utilized to only look for reaction between different molecules to stop chain cyclization. This was an assumption that chains would not cyclize during polymerization and was being tested since this level of control with MD polymerization is recently available with the *fix bond/react* command. The polymerization temperature used was 633K for 1.5ns and polymerization behavior was tracked using Carothers polycondensation reaction equation. Five replicates of amorphous crystalline PEKK were built and the average conversion factor was 93.95%. The experimental molecular weight of PEKK is not published and could not be used to validate this conversion factor, thus it is assumed that this conversion factor is like that of experimental amorphous PEKK. Crystalline models of Form 1, Form 2i, and Form 2ii were also modeled [1]. The crystalline forms presented there are for a pure PEKK T/I ratio of 100/0, however PEKK T/I ratio 70/30 is desired. It was assumed that crystalline PEKK T/I ratio of 70/30 had similar crystalline unit cells of its 100/0 counterpart. To build the crystalline PEKK models a chain of 70/30 was polymerized using *fix bond/react* with the optional *inter* flag to produce a single chain. The chain was then straightened in an NPT environment at 1000K and 1000atm. The straighten chain was then reacted across the bonded periodic direction to produce a single chain orthorhombic cell. The single chain orthorhombic cell was then duplicated using the LAMMPS *replicate* command and the cell dimensions were set to each of the known PEKK T/I 100/0 cell dimensions. Once both the amorphous and crystalline phases were built, they were subjected to simulations to predict Young's, modulus, Poisson's ratio, Yield strength, shear Modulus, glass transition temperature (Tg), coefficient of thermal expansion (CTE), and thermal conductivity. The material properties will then be used in higher length scale models to homogenize the MD predicted properties.

PEEK was modeled using the OPLS force field initially and converted to the ReaxFF force field for property prediction. All PEEK modeling was performed using LAMMPS simulation software available at that time. Reactive force fields are needed to accurately predict elastic properties since they have the ability for bond scission. During the time the when the work on PEEK was performed, the main reactive force field available was ReaxFF. However, it is difficult to model bond creation in ReaxFF and is still ongoing research in the MD community. This means the polymerization of PEEK had to occur in a fix bond force field like OPLS using the LAMMPS command *fix bond/create.* Which differs from the LAMMPS command used in PEKK modeling of *fix bond/react*, mainly by the level of control and complexity or reactions that can be created. Amorphous and crystalline phases of PEEK were also modeled separately with the intention to homogenize in the available MAC/GMC. The amorphous phase was built like PEKK, but with the *fix bond/create* command and then converted to ReaxFF for property prediction. The crystalline phase of PEEK modeled was smaller then PEKK and did not require to be polymerized and straighten like the PEKK models. The crystalline phase of PEEK was initialized on OPLS and then converted to ReaxFF for property predictions. The MD predicted properties of PEEK were Young's modulus, Poisson's ratio, shear modulus, and later CTE [19]. For complete details on all the MD modeling of PEEK and PEKK, the reader is referred to Refs. [18, 19, 27].

The PEEK properties were averaged from statistical data calculated using MD [18]. Values for Young's modulus E_a, shear modulus G_a, and Poisson's ratio v_a of the amorphous phase or PEEK are presented in Table 2, respectively. The orthotropic properties of the crystalline PEEK (Young's modulus E_{ii}, shear modulus G_{ij}, and Poisson's ratio v_{ij}) are given in Table 3. The subscripts *i, j* represent the direction at Level 3 (see Fig. 2).

More recently, properties of PEKK were predicted with MD for PEKK 7002 which has a terephthalic acid (T) or isophthalic acid (I) ratio of 70/30 [27]. The amorphous values are given in Table 4 including the CTE α_a and thermal conductivity κ_a. Unlike PEEK, crystalline PEKK can exist in various forms, i.e., Form 1, Form 2i, and Form 2ii. Since it was uncertain what crystalline forms existed in the material used to produce the data for validation, the averages of values (see Table 3) for the properties of the different forms are used in the predictions here [3]. Only the longitudinal values of thermal conductivity κ_{11} for the crystalline PEKK unit cells were calculated using MD [27]. Since thermal conductivity is affected by bond stiffness and van der Waals interactions, the thermal conductivity in transverse directions κ_{22}, κ_{33} in Table 4 is estimated by scaling the longitudinal thermal conductivity κ_{11} by the ratio of the stiffnesses E_{22}/E_{33}. The CTE in Table 4 was calculated as a volumetric quantity; so, the same value is used for all directions in the crystalline PEKK.

Table 2. Thermoelastic constituent properties of amorphous PEEK and PEKK obtained from MD [18, 19, 27].

Property	PEEK	PEKK
E_a (GPa)	3.62 [18]	1.87 [27]
G_a (GPa)	1.28 [18]	0.67 [27]
ν_a	0.38 [18]	0.43 [27]
α_a (1/°C)	6.07E-5 [19]	1.13E-4 [27]
κ_a (W/(m-K))	-	0.43 [27]

Table 3. Elastic constituent properties of crystalline PEEK and PEKK obtained from MD [18, 27].

Property	PEEK [18]	PEKK [27]
E_{11} (Gpa)	117.0	163.47
E_{22} (Gpa)	8.51	2.88
E_{33} (Gpa)	8.37	2.88
G_{23} (Gpa)	1.52	1.08
G_{13} (Gpa)	1.92	1.09
G_{12} (Gpa)	0.69	0.93
ν_{23}	0.5	0.32
ν_{13}	1.92	0.32
ν_{12}	0.69	0.32

Table 4. Averaged thermoelastic constituent properties of the different forms crystalline PEEK and PEKK [19, 27].

Thermal Property	α_{11} (1/°C)	α_{22} (1/°C)	α_{33} (1/°C)	κ_{11} (W/(m-K))	κ_{22} (W/(m-K))	κ_{33} (W/(m-K))
PEEK [19]	4.29E-5	1.44E-4	-7.33E-6	-	-	-
PEKK [27]	8.50E-5	8.50E-5	8.50E-5	2.80	0.049	0.049

IV. Model Verification and Convergence Studies

A. Verification of Crystallinity

To determine the discretization requirements at the highest scale, it must be verified that the target total crystallinity χ is met. Figure 4 shows the error in total crystallinity as a function of number of subcells N in each global direction (the total size of the RUC is N x N x N) for the models with a spherical spherulite and a cubic spherulite. The error in crystallinity in the spherical model drops below 1% at 32 subcells, and the cubic model converges towards a 3% error in crystallinity. The convergence of the spherical model oscillates because the voxelized sphere does not identically match the volume of a true sphere. The discrepancy between the trends in local crystallinity is attributed to differences among the algorithms used to determine the local crystallinity v_c in the subcells, which is set in the Level 1 crystallite RUC (see Fig. 2).

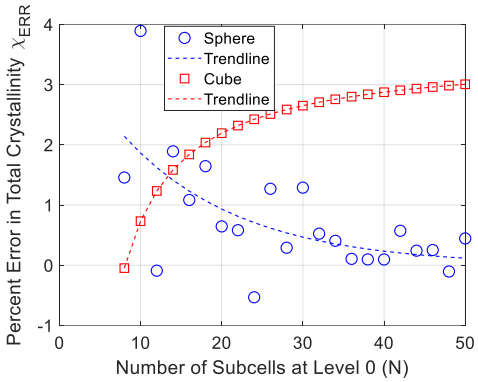

Fig. 4 Percent error in total volume fraction of crystalline phase in MsRM models as function of subcell grid refinement at Level 0.

Figure 5 shows the local crystallinity as a function of distance from the center of the RUCs. The spherical model assumes the spherulite core has a crystal volume fraction of 0.85 and the crystallinity of the spherulite, not including the surrounding amorphous matrix, is assigned in such a manner to satisfy the target crystallinity with the caveat that the local crystallinity must increase as a function of radial distance from the center of the RUC. The local subcell crystallinity is calculated in a piecewise linear fashion, subjected to the aforementioned constraints. The cubic model assumes that the boundaries of the spherulite have zero crystallinity, and the volume fraction of the crystalline phase in the subcells is set using a linear equation that is predetermined based on the volume fraction requirements of the cubic spherulite needed to meet the over target crystallinity. This results in a lower crystallinity in the core of the cube, 0.675. Figure 6 shows a midplane slice of the RUCs. The color contour represents the local crystallinity of the subcells for the RUCs with a target crystallinity χ = 0.288.

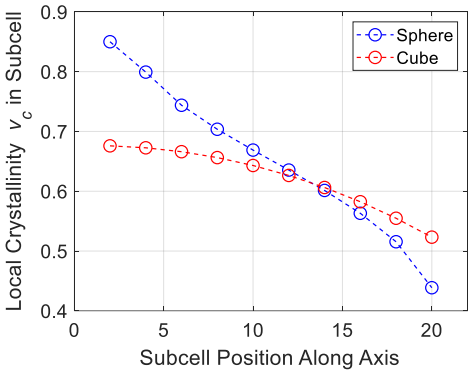

Fig. 5 Local crystallinity in the subcells of RUCs with spherical and cubic spherulites and converged crystallinity at N=20 as a function of distance from the center along a global material coordinate axis.

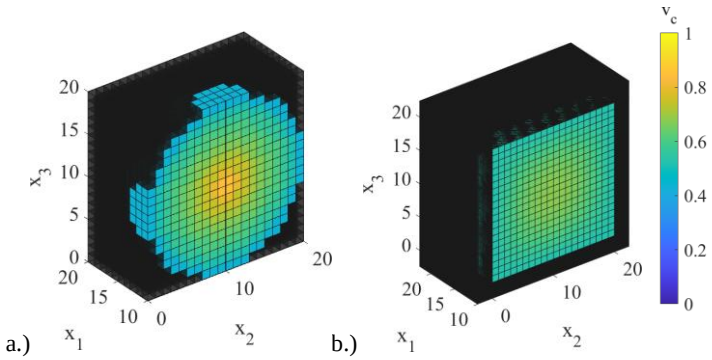

Fig. 6 Geometry of RUCs with converged total crystallinity χ =0.288 at N=20. The color contour represents the local crystallinity in the subcells. a.) Spherical spherulite. b.) Cubic spherulite.

B. Property Convergence Studies

The discretization of the RUC must be sufficient to not only satisfy target crystallinity but also dense enough such that the analysis results to not significantly change with further refinements of the subcell grid. Since the aim of this work is the prediction of the effective linear properties of bulk thermoplastics, convergence studies on the local fields are beyond scope. Typically, the discretization density requirements for convergence of local fields are beyond those for effective properties but would be needed for accurate prediction of nonlinear material behavior.

Figure 7 shows the effective elastic properties of the RUCs of PEEK and PEKK as a function of the number of subcells *N* in each direction at Level 0. The black and blue circular points represent the results of the spherical model, while the red and green square data is from the results of the cubic model, respectively. Convergence was deemed to occur at the value of *N* which resulted in properties that exhibited less than a 2.5% difference, as compared to the most refined models (*N*=50), and beyond which no further model refinement exhibited more than 2.5% difference. This convergence threshold of 2.5% difference was chosen to ensure consistency in the properties across the models, while avoiding keeping the computational cost of the models tractable. The CTE, as a function of subcell refinement, is displayed in Fig. 8 for PEKK (MD predictions for PEEK constituent properties were not obtained). Only results for GMC are presented because homogenization of the CTE using triply periodic HFGMC has not been implemented in NASMAT. It can be inferred, the CTE is directly correlated to the total crystallinity as the trends in Fig. 8 follow those in Fig 4. Note, the curve for the cubic inclusion in Fig. 8 is inverse to that in Fig. 4 because the percent difference is calculated from the data of the most refined model (α at N = 50), as opposed to the known value (χ).

The results of the convergence study for the elastic properties are summarized in Table 5. GMC models exhibit faster convergence than HFGMC models, and the cubic models converge faster than the spherical, while the PEEK and PEKK models produce converged results with similar refinement. Based on the data in Table 5, the spherical and cubic models will be discretized with N = 32 subcell in each direction. The total number of subcells, across three scales, in each prediction analysis was 16,384, and the runtimes were less than five minutes on a single cpu.

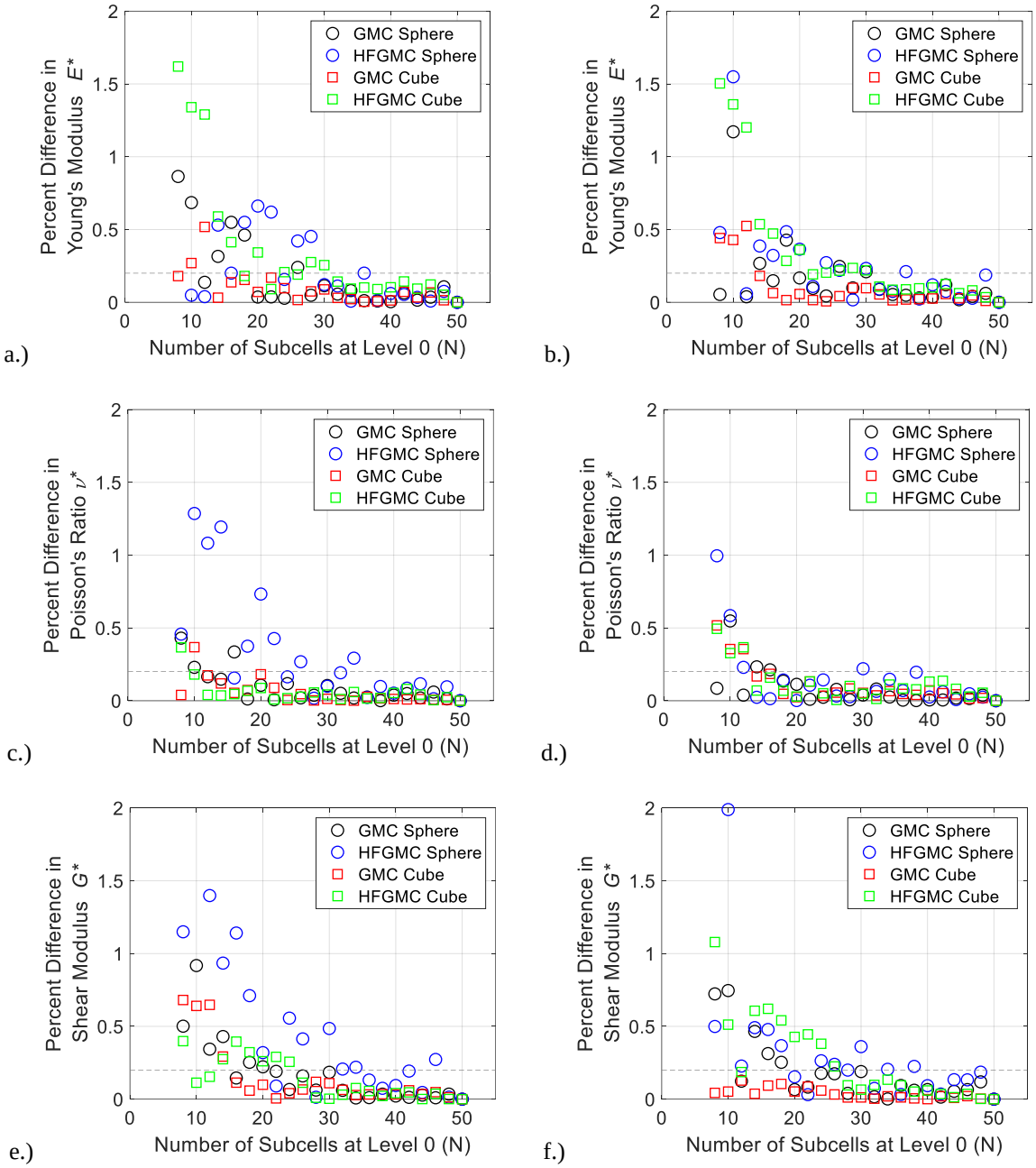

Fig. 7 Precent difference (as compared to N=50) in elastic properties of 30% crystalline PEEK and PEKK predicted with NASMAT as function of subcell grid refinement at Level 0. The gray dashed line represents the 2.5 difference convergence threshold. a.) Young's Modulus of PEEK. b.) Young's Modulus of PEKK. c.) Poisson's ratio of PEEK. d.) Poisson's Ration of PEKK. e.) Shear Modulus of PEEK. d.) Shear Modulus of PEKK.

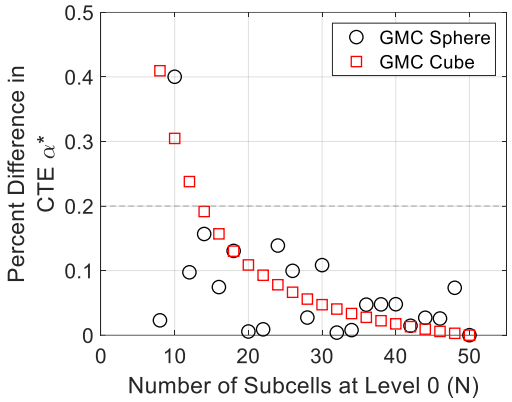

Fig. 8 Percent difference (as compared to N=50) in CTE of 30% crystalline PEKK predicted with NASMAT as function of subcell grid refinement at Level 0. The gray line represents the threshold for convergence.

Table 5. Number of subcells *N* required in each model for convergence of elastic properties.

Property	GMC Sphere (PEEK/PEKK)	HFGMC Sphere (PEEK/PEKK)	GMC Cube (PEEK/PEKK)	HFGMC Cube (PEEK/PEKK)
E	28/32	38/38	14/14	32/32
v	18/20	36/32	12/14	10/14
G	22/20	48/40	16/8	26/28

V. Prediction of Thermoelastic Properties as a Function of Crystallinity

The thermoelastic properties as a function of crystallinity for PEEK and PEKK, predicted with the four models described in Table 1 using NASMAT and discretized with $N = 32$ are presented in this section. Experimental data available in the open literature on these materials is extremely limited, but the computational results are compared to experiments when available.

The effective Young's modulus E predicted as a function of χ is shown in Fig. 9 for PEEK (Fig. 9a); the results from GMC models are bounded by the test data [2]. However, the HFGMC models predicted a large, nonlinear increase in stiffness as the crystallinity was increased, resulting in an over prediction of the effective Young's modulus. The shape of the geometry of the spherulite seems to have minimal influence on the Young's modulus. This indicates it is primarily influenced by the crystallinity, and not the morphology, of the spherulite. Moreover, HFGMC is sensitive to the arrangement of the inclusions. Therefore, a study on spherulite packing and morphology is needed to understand these effects.

The predictions of the effective Young's modulus of PEKK exhibit significant error, as shown in Fig. 9b. It should be noted, the experimental data presented in Fig. 9b is an amalgamation of data for three different forms of PEKK (6002, 7002, 8002), whereas the predictions are strictly for PEKK 7002 [3]. The simulation results are insensitive to the shape of the spherulite. It is expected the shape of the spherulite would have a more pronounced effect on the prediction of the local fields. The data for the Young's modulus was normalized by the value for amorphous PEKK in Fig. 10. The normalized data predicted by the GMC models matches well for all values of crystallinity with

experiment. This indicates that there may be some discrepancy between the amorphous modulus predicted with MD and experiment.

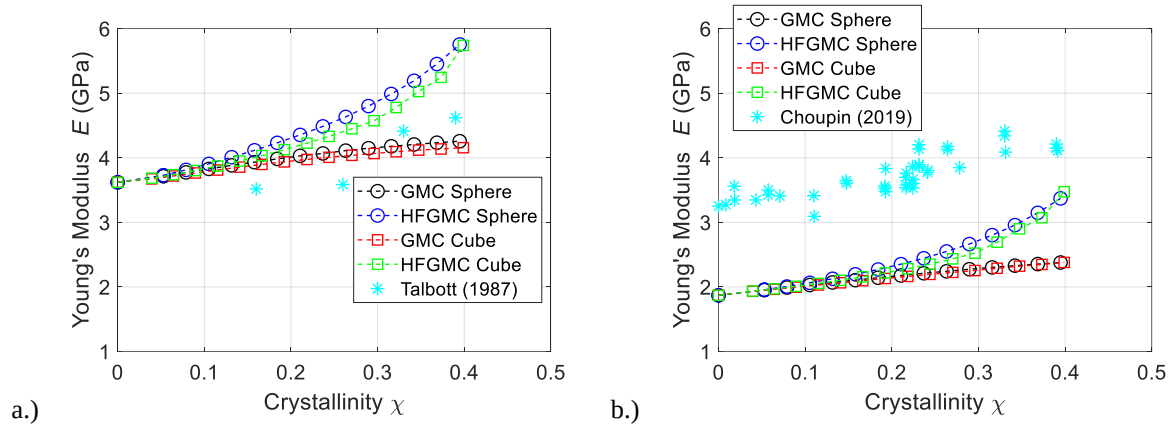

Fig. 9 Predicted effective Young's modulus as a function of crystallinity compared to available experimental data [2, 3]. a.) PEEK. b.) PEEK.

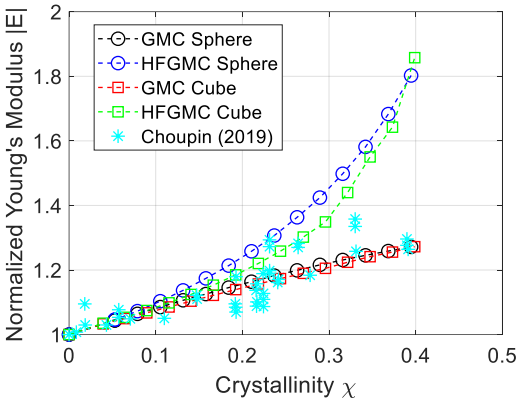

Fig. 10 Predicted effective Young's modulus of PEKK, normalized by amorphous properties, as a function of crystallinity compared to available experimental data [3].

There are two main reasons that the predicted value for the Young's modulus of the amorphous PEKK are underpredicted, as compared to experimental. The first reason being, it was assumed that no chain cyclization would occur in the experimental polymerization, and MD polymerization protocols were used to stop chain cyclization. The lack of chain cyclization or chain looping means that the chain unwrapping mechanisms are completely reliant on IFF-R's angle and torsional parameters. The reason that the MD models were polymerized to stop chain cyclization was to impede the chaining together of possible cyclized chains. However, it also stopped the cyclization completely. If chains were to cyclize the chain unwrapping mechanism that produces the stress-strain behavior would be reliant on IFF-R's bond, angle, and torsional parameters which would significantly increase the predicted modulus. The second possible reason that the MD simulations predict a low modulus is that it was assumed a conversion factor of about 93.9% was not high enough to produce a molecular weight distribution that is comparable to experimental molecular weight distribution. For thermosetting resins that undergo polycondensation reactions like PEKK, it is not uncommon to see conversion factors nearing 99%. However, this data on thermoplastic resins is limited in the open literature.

Figure 11 shows the prediction results for the effective shear modulus G of PEEK and PEKK. Only limited experimental data was obtained for PEEK and shown in Fig. 11.a. The results from the GMC models match well with the test data, and the HFGMC models exhibit errors similar to those for the Young's modulus.

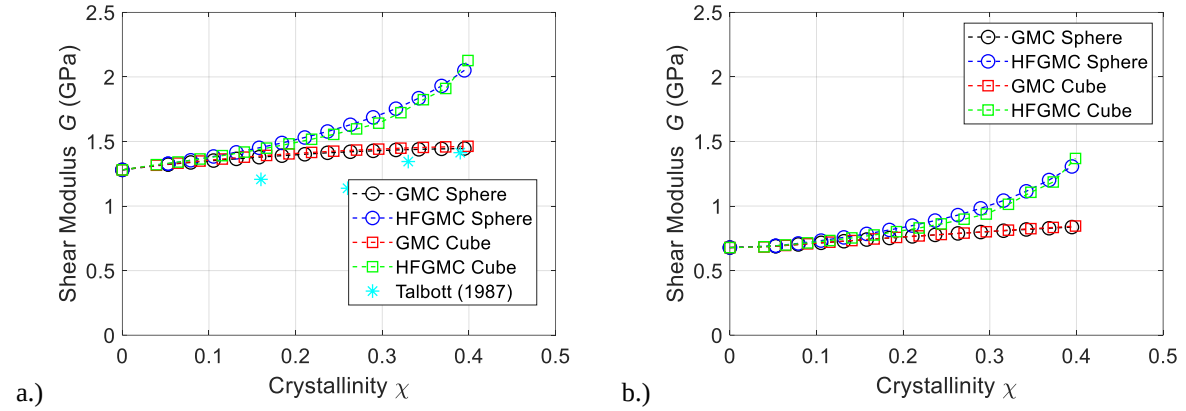

Fig. 11 Predicted effective shear modulus as a function of crystallinity compared to available experimental data [2]. a.) PEEK. b.) PEKK.

Predictions of the Poisson's ratios ν of PEEK and PEKK as a function of crystallinity are plotted in Fig. 12. No experimental data was found for ν in the literature. The micromechanics theory used at Level 0 affected the predictions for the Poisson's ratio of PEEK, but not PEKK, most likely because of the large mismatch between ν_{13} of the crystalline PEEK and the Poisson's ratio of the amorphous phase as well as of the other directions for the crystal. The trend predicted for PEEK and PEKK are opposite which also can be attributabed to the large ν_{13} value predicted for PEEK with MD [18].

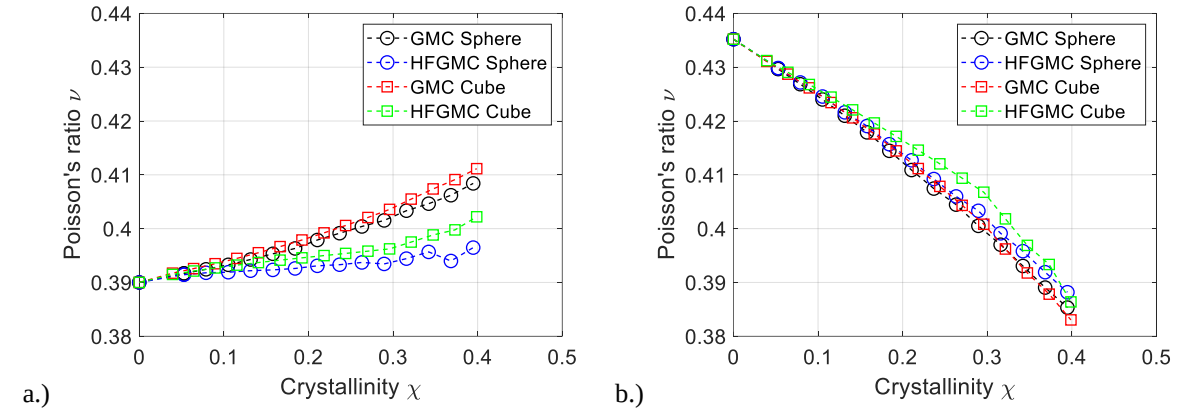

Fig. 12 Predicted effective Poisson's ratio as a function of crystallinity. a.) PEEK. b.) PEKK.

Even more limited than the data in the literature available for the elastic properties, is the data for the thermal properties. Homogenization of the CTE for a triply periodic RUC using HFGMC is not implemented in NASMAT. Thus, predictions using only GMC (at Level 0) for PEEK and PEKK are given in Fig. 13. Figure 13a shows the predicted CTE as a function of crystallinity compared to experimental data [34, 35]. The models exhibited between ~18-27% error compared to Ref. [35] at 0 and ~0.35 crystallinity. The predictions were in better agreement (< 2%) with the more recent data for CTE as a function of processing time; crystallinity was not reported [35]. The experimental data was obtained from a datasheet produced by Arkema and did not list the crystallinity of the material [34]. Moreover, this data was presented as the average of measurements taken between -100 ^{o}C to T_g and T_g to 300 ^{o}C. That said, the modeling predictions are bounded by the two data points. The simulation results are only sensitive to the crystallinity, not the morphology, because an isotropic volumetric CTE was used as input [27]. For both materials the predicted influence of crystallinity on the CTE is small which is consistent with previous predictions from a multiscale model for PEEK [19].

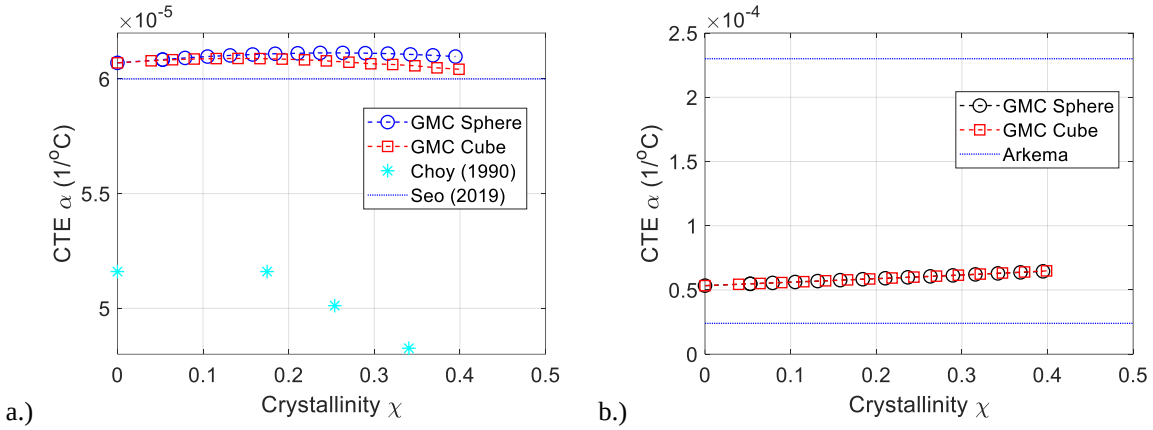

Fig. 13 Predicted effective CTE as a function of crystallinity compared to experimental data [33-36]. a.) PEEK. b.) PEKK. Experimental data average values measured from -100 ºC to T_g and T_g to 300 ºC.

Finally, the predictions for the effective thermal conductivity κ as a function of crystallinity are given in Fig. 14. Vector-based constitutive laws require the high fidelity homogenization, presented in Section II, at every scale. Therefore, the results in Fig. 14 were generated using a single method. Experimental data available in the open literature for thermal conductivity of PEKK is extremely sparse, and none was obtained for PEEK. The thermal conductivity of PEKK was reported as 2.4 W/(m-K), but no information on crystallinity or crystalline forms was given [34]. The error between the predictions and experimental data ranges from ~39-79%. The shape of the spherulite had a minimal effect on the effective thermal conductivity calculations, and the models predicted that conductivity goes down as crystallinity increases. More experimental data on both the CTE and thermal conductivity is needed before any conclusions can be drawn about the multiscale model.

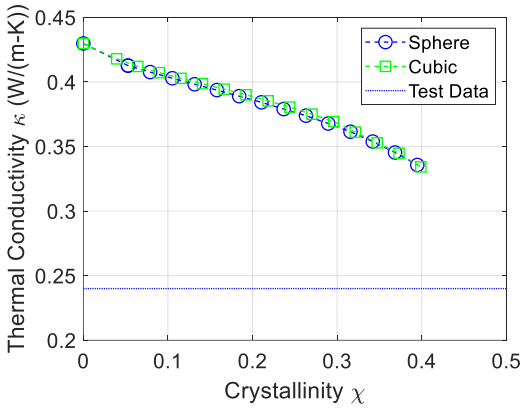

Fig. 14 Predicted effective thermal conductivity as a function of crystallinity for PEKK compared to experimental data [37].

The total number of subcells, across three scales, in each multiscale prediction analysis was 16,384. Each analysis was run on a single processor on a high performance computing cluster that consisted of three Intel Xeon CPU E5-2698 v4 at 2.20 GHz nodes, each with 450 GB of shared memory and 40 processors. Analysis times ranged from ~40-180 sec., ~185-315 sec., ~90-220 sec. for GMC, HFGMC and vectorized HFGMC, respectively.

VI. Conclusion

A multiscale model was developed for semi-crystalline thermoplastics using the MsRM framework implemented in NASMAT. Several models were evaluated by changing the shape of the spherulite inclusion (cubic and spherical) as well as the analysis methods used at the highest scale (GMC and HFGMC). Inputs for properties of the amorphous and crystalline phases used as the base constituents for the models were obtained from MD simulations. Therefore, the predictions presented here were obtained entirely using virtual data.

Prior to predicting the effective thermoelastic properties of PEEK and PEKK studies were performed to determine the level of discretization necessary to obtain converged properties. A subcell grid density using $N = 32$ subcells in each direction was deemed sufficient.

Model predictions of the thermoelastic properties of PEEK and PEKK as function of crystallinity were in good agreement with the limited experimental data available in the literature. In general, the models that utilized HFGMC at the highest scale over predicted the stiffness as the crystallinity was increased. Due to the lack of normal-shear coupling, the homogenized stiffness calculated with GMC are controlled by the "weakest link" along any given row or column. The effective properties were not substantially affected by the shape of the spherulite. However, the HFGMC results would be affected by changes in the morphology of the microstructure. It is expected that, accuracy in the local fields needed for non-linear predictions are more sensitive to the micromechanics theory used. Significant error in the results for Young's modulus PEKK was observed. However, when the data is normalized by the properties for the amorphous phase, the results match closely with experimental data. The error in the amorphous properties calculated using MD is likely due to the absence of chain cyclization and low conversion factor in the simulations. Test data on the CTE of thermoplastics PEEK and PEKK is very limited, but the modeling predictions were bounded by the data.

With the validated multiscale model in place additional studies can be performed including sensitivity of the effective properties on morphological effects of the semi-crystalline microstructure of thermoplastics such as the packing of the spherulites and ratio of inter-spherulite amorphous matrix to crystalline phases. Damage and plasticity material models can be used to predict the non-linear behavior of the thermoplastics. In addition, crystallization kinetics can be used in conjunction with model to perform processing simulations. Finally, this model can be integrated into a model for fibrous composites to perform multiscale simulations of fiber reinforced thermoplastic composites considering both the fiber architecture and matrix microstructure.

Acknowledgments

Dr. Pineda's contributions were sponsored by the Office of Naval Research (ONR) under Interagency Agreement SAA3-1697. Mr. Husseini's contributions were funded by a NASA Space Technology Graduate Research Opportunity (NSTGRO) Grant Number #80NSSC21K1285. Dr. Bednarcyk would like to thank the NASA Thermoplastics Development for Exploration Applications (TDEA) project for their support. Mr. Kemppainen would like to acknowledge the NASA Internship Project (NIP).

References

[1] Pérez-Martín, H., Mackenzie, P., Baidak, A., Ó Brádaigh, C. M., and Ray, D. (2021). "Crystallinity Studies of PEKK and Carbon Fibre/PEKK Composites: A Review," *Composites Part B*, Vol. 223, 109127.

[2] Talbott, M. F., Springer, G. S., and Berglund, L. A. (1987). "The Effects of Crystallinity on the Mechanical Properties of PEEK Polymer and Graphite Fiber Reinforced PEEK," *Journal of Composite Materials*, Vol. 21, pp. 1056-1080.

[3] Choupin, T., Debertrand, L., Fayolle, B., Régnier, G., Paris, C., Cin quin, J., and Brulé, B. (2019). "Influence of thermal history on the mechanical properties of poly(ether ketone ketone) copolymers," *Polymer Crystallization*, 2(6), pp. 1-8.

[4] Bandyopadhyay, A., Valavala, P. K., Clancy, T. C., Wise, K. E., and Odegard, G. M. (2011). "Molecular Modeling of Crosslinked Epoxy Polymers: The Effect of Crosslink Density on Thermomechanical Properties," *Polymer*, Vol. 52, No. 11, pp. 2334-2452.

[5] Odegard, G. M., Jensen, B. D., Gowtham, S., Wu, J., He, J., and Zhang, Z. (2014). "Predicted mechanical response of crosslinked epoxy using ReaxFF," *Chemical Physics Letters*, pp. 175-178.

[6] Chapman, T.J., Gillespie, Jr., J.W., Pipes, R.B., Manson, J.-A. E., and Seferis, J.C., "Prediction of Process-Induced Residual Stresses in Thermoplastic Composites" *Journal of Composite Materials*, 24, 1990, pp. 616-643.

[7] Ogale, A.A. and McCullough, R.L. "Influence of microstructure on elastic and viscoelastic properties of polyether ether ketone" *Composite Science and Technology*, 30, 1987, pp. 185-201.

[8] Guan, X. and Pitchumani, R. "A Micromechanical Model for the Elastic Properties of Semicrystalline Thermoplastic Polymers" *Polymer Engineering and Science*, 44, 2004, pp. 433-451.

[9] Bédoui, F., Diani, J., Régnier, G., and Seiler, W. "Micromechanical modeling of isotropic elastic behavior of semicrystalline polymers" *Acta Materialia*, 54, 2006, pp. 1513-1523.

[10] Diani, J., Bédoui, F., and Régnier, G. "On the relevance of the micromechanics approach for predicting the linear viscoelastic behavior of semi-crystalline poly(ethylene)terephtalates (PET)" *Materials Science and Engineering A*, 475, 2008, pp. 229-234.

[11] Gueguen, O., Ahzi, S., Belouettar, S., and Makradi, A. "Comparison of micromechanical models for the prediction of the effective elastic properties of semicrystalline polymers: Application to polyethylene" *Polymer Science Series A*, 50, 2008, pp. 523-532.

[12] Glüge, R., Altenbach, H., Kolesov, I., Mahmood, N., Beiner, M., and Androsch, R. "On the effective elastic properties of isotactic polypropylene" *Polymer*, 160, 2019, pp. 291-302.

[13] van Dommelen, J.A.W., Poluektov, M., Sedighiamiri, A., and Govaert, L.E. “Micromechanics of semicrystalline polymers: Towards quantitative predictions” *Mechanics Research Communications*, 80, 2017, pp. 4-9.
[14] Hsia, K.J, Xin, Y.B., and Lin, L. “Numerical simulation of semi-crystalline nylon 6: elastic constants of crystalline and amorphous parts”, *J. Mater. Sci.*, 29, 1994, 1601–1611.
[15] Doyle, M.J. “On the effect of crystallinity on the elastic properties of semicrystalline polyethylene”, *Polym. Eng. Sci.*, 40, 2000, pp. 330–335.
[16] Poluektov, M., van Dommelen, J.A.W., Govaert, L.E., Yakimets, I., and Geers, M.G.D. “Micromechanical modelling of poly(ethylene terephthalate) using a layered two-phase approach”, *J. Mater. Sci.*, 48, 2013, pp. 3769–3781.
[17] Jin, L. Ball, J., Bremner, T., and Sue, H.-J. “Crystallization behavior and morphological characterization of poly(ether ether ketone)” *Polymer*, 55, 2014, pp. 5255-5265.
[18] Pisani, W. A., Radue, M. S., Chinkanjanarot, S., Bednarcyk, B. A., Pineda, E. J., Waters, K., Pandey, R., King, J. A., and Odegard, G. M. (2019). “Multiscale Modelling of PEEK using Reactive Molecular Dynamics Modeling and Micromechanics,” *Polymer*, Vol. 163, pp. 96-105.
[19] Kashmari, K., Deshpande, P., Patil, S., Maiaru, M., and Odegard, G. M. (2022). “A multiscale approach to investigate the effect of temperature and crystallinity on the development of residual stresses in semicrystalline PEEK,” *American Society for Composites 37th Technical Conference*, 19-21 September, Tucson, AZ.
[20] van Duin, A. C. T., Dasgupta, S., Lorant, F., and Goddard, W. A. (2001). "ReaxFF: A Reactive Force Field for Hydrocarbons," *The Journal of Physical Chemistry A*, Vol. 105, No. 41, pp. 9393-9409.
[21] Bednarcyk, B. A., and Arnold, S. M. (2002). "MAC/GMC 4.0 User's Manual - Keywords Manual," *NASA TM-2002-212077/Vol2*.
[22] Aboudi, J., Arnold, S. M., and Bednarcyk, B. A. (2013). *Micromechanics of Composite Materials: A Generalized Multiscale Analysis Approach*, Oxford, UK: Elsevier.
[23] Pisani, W. A., Newman, J. K., and Shukla, M. K. (2021). “Multiscale Modeling of Polyamide 6 Using Molecular Dynamics and Micromechanics,” *Industrial & Engineering Chemistry Research*, Vol. 60, No. 37, pp.13604-13613
[24] Bednarcyk, B. A., Pineda, E. J., Ricks, T. M., and Mital, S. K. (2021). “Progressive Damage Response of 3D Woven Composites via the Multiscale Recursive Micromechanics Solution with Tailored Fidelity,” *American Society for Composites 36th Technical Conference*, 20-22 September 2021, Virtual Conference.
[25] Pineda, E. J., Bednarcyk, B. A., Ricks, T. M., and Henson, G. (2021). “Efficient Multiscale Recursive Micromechanics of Composites for Engineering Applications,” *International Journal for Multiscale Computational Engineering*, 19(4), 77-105.
[26] Bednarcyk, B. A., Aboudi, J., and Arnold, S. M., (2017). “Micromechanics of composite materials governed by vector constitutive laws,” *International Journal of Solids and Structures*, Vol. 110-111, pp. 137-151.
[27] Kemppainen, J.D., Varshney, V., Pineda, E. J., and Odegard, G. M. (2022). Thermo-mechanical property prediction of amorphous/crystal PEKK via molecular dynamics. NASA-TM-20220018678 (in press).
[28] Pineda, E. J., Bednarcyk, B. A., Ricks, T. M., Farrokh, B., and Jackson, W. C. (2022). “Multiscale Failure Analysis of a 3D Woven Composite Containing Manufacturing Voids and Disbonds,” *Composites Part A: Applied Science and Manufacturing*, 156(2022) 106844.
[29] Bednarcyk, B.A., Ricks, T.M., Pineda, E.J., Murthy, P., Mital, S., Hu, Z., and Gustafson, P.A. (2022). “Thermal Conductivity of 3D Woven Composite Thermal Protection System Materials via Multiscale Recursive Micromechanics,” *2022 AIAA SciTech Forum*, 3-7 January 2022, San Diego, CA.
[30] Ricks, T.M., Pineda, E.J., Bednarcyk, B.A., and Arnold, S.M. (2021) “Progressive Failure Analysis of 3D Woven Composites via Multiscale Recursive Micromechanics,” *AIAA SciTech Forum* (virtual), Jan. 11-21, 10.2514/6.2021-0702.
[31] Pahr, D., and Arnold, S. M. (2002). “The applicability of the generalized method of cell for analyzing discontinuously reinforced composites,” *Composites Part B: Engineering*, 33 (2), pp. 153-170.
[32] Choupin, T., Fayolle, B., Régnier, G., Paris, C., Cinquin, J., and Brulé, B. (2017). “Isothermal crystallization kinetic modeling of poly(etherketoneketone) (PEKK) copolymer,” *Polymer*, 111, pp. 73-82.
[33] Arkema. (2012). KEPSTAN by Arkema Technical Data – 7000 Series.
[34] Choy, C. L., Leung, W. P., and Nakafuku, C. (1990). “Thermal expansion of poly (ether-ether- ketone) (PEEK),” *Journal of Polymer Science: Part B: Polymer Physics*, 28, pp. 1965-1977.
[35] Seo, J., Gohn, A. M., Dubin, O., Takahashi, H., Hasegawa, H., Sato, R., Rhoades, A. M., Schaake, R. P., and Colby, Ralph H. (2019). “Isothermal crystallization of poly(ether ether ketone) with different molecular weights over a wide temperature range,” *Polymer Crystallization*, 2(1), e10055.
[36] Polyetherketoneketone (PEKK) datasheet. (2022). *https://matmatch.com/materials/mbas044-polyetherketoneketone-pekk-*.